ACS APPLIED MATERIALS & INTERFACES

Research Article

www.acsami.org

Predicting the Interface Morphologies of Silicon Films on Arbitrary Substrates: Application in Solar Cells

Vladislav Jovanov,[†] Xu Xu,[‡] Shailesh Shrestha,[†] Melanie Schulte,[‡] Jürgen Hüpkes,[‡] and Dietmar Knipp*,[†]

[†]Research Center for Functional Materials and Nanomolecular Science, Electronic Devices and Nanophotonics Laboratory, Jacobs University Bremen, 28759 Bremen, Germany

[‡]Institut für Energie- und Klimaforschung, IEK5−Photovoltaik, Forschungszentrum Jülich, 52425 Jülich, Germany

ABSTRACT: A three-dimensional model that predicts the interface morphologies of silicon thin-film solar cells prepared on randomly textured substrates was developed and compared to experimental data. The surface morphologies of silicon solar cells were calculated by using atomic force microscope scans of the textured substrates and the film thickness as input data. Calculated surface morphologies of silicon solar cells are in good agreement with experimentally measured morphologies. A detailed description of the solar cell interface morphologies is necessary to understand light-trapping in silicon single junction and micromorph tandem thin-film solar cells and derive optimal light-trapping structures.

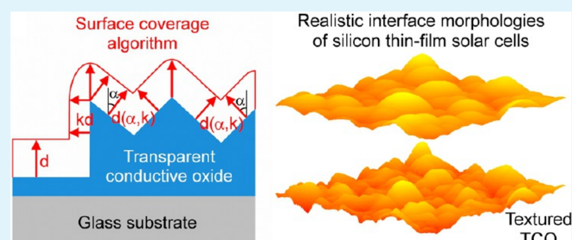

KEYWORDS: *light-trapping, surface morphology evolution, thin-film solar cells, interface prediction*

INTRODUCTION

Photon-management or light-trapping is crucial for achieving silicon thin-film solar cells with high energy conversion efficiency. Efficient light-trapping in silicon thin-film solar cells is realized by texturing the front or back contact. Randomly textured transparent conductive oxides (TCO) are widely used as front contacts to achieve light-trapping in superstrate (p-i-n) configuration solar cells.[1−10] Light-trapping in substrate (n-i-p) configuration solar cells is achieved by texturing the back contact.[11−17] When depositing amorphous or microcrystalline silicon on textured substrates, the surface textures propagate through the thin-film solar cell leading to a solar cell with textured front and back contact. Experimental results and optical simulations show that solar cells with both contacts textured exhibit high short circuit currents.[14,18] Most publications in the literature assume that surface textures propagate unchanged through the thin-film solar cell.[18−21] However, experimental measurements reveal that surface textures are significantly affected by the solar cell deposition process leading to different front and back contact textures.[9,22−27]

Determining the interface morphologies of silicon solar cells deposited on textured substrates allows for deriving new strategies to optimize and improve light-trapping. The interface morphologies can be measured by atomic force microscopy (AFM). However, complex aligning procedures are required to measure the corresponding front and back contact texture. As an alternative, cross-sectional scanning electron microscopy (SEM) images can be used.[9,23−27] However, cross sectional SEM images can be used only for two-dimensional (2D) textured substrates, such as line-gratings or three-dimensional (3D) textured substrates with periodical surface textures and radial symmetry. This manuscript describes a simple approach to predict the interface morphologies of amorphous and microcrystalline silicon thin-film solar cells deposited on textured substrates using plasma enhanced chemical vapor deposition (PECVD). The approach is demonstrated for silicon solar cells deposited on randomly textured TCO. However, the same approach can be used to determine the interface morphologies of silicon single junction and micromorph tandem solar cells deposited on different textured substrates, including coaxial nanowire solar cells or textured glass substrates.[1,4,12,22,24,25]

METHODS

Modeling Interface Morphology. Light-trapping in silicon thin-film solar cells is influenced by the front and back contact morphology. The front contact textures should increase scattering/diffraction of the incident light, while minimizing reflection losses. The front contact textures in superstrate configuration solar cells are determined by the fabrication process of the TCO layer. Sputtered and etched zinc oxide (ZnO) films exhibit craterlike features, while pyramidlike features are observed for ZnO films prepared by low pressure chemical vapor deposition and tin oxide films fabricated by atmospheric pressure chemical vapor deposition.[2−9] The interface and back contact morphology are determined by the surface textures of TCO and the silicon film formation. Consequently, significant differences between the front and back contact morphology are observed (Figure 1b).

Figure 1 exhibits cross sections of typical amorphous silicon thin-film solar cells prepared on commercial Asahi U substrate.[3−6] The common approach to model thin film solar cells by using identical front and back contact morphology is shown in Figure 1a. Figure 1b depicts the cross section of an amorphous silicon solar cell based on experimental measurements. The back contact morphology determines the optical losses and scattering properties of the metal back reflector. Hence, an

Received: April 19, 2013
Accepted: July 15, 2013
Published: July 29, 2013

 © 2013 American Chemical Society

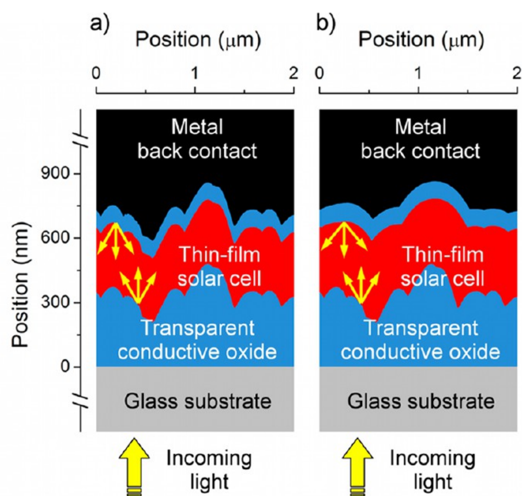

Figure 1. Cross-section of amorphous silicon solar cell deposited on Asahi U substrate using (a) common model of the back contact morphology and (b) experimentally measured back contact morphology.

accurate description of the back contact textures is required to create a realistic optical model and determine the optimal light-trapping structures.

Silicon solar cells are commonly deposited by a PECVD process.[3−15] PECVD growth conditions range from chemical vapor deposition (CVD) to physical vapor deposition (PVD) conditions.[28,29] PVD-like growth conditions result in films with high density of electronic defects.[28,29] On the other hand, CVD-like growth conditions result in uniform films with low defect density.[28,29] For solar cell applications, silicon films with low defect density are required and CVD-like growth conditions are necessary.[28−30] CVD-like growth conditions exhibit a low sticking coefficient, resulting in an excellent surface coverage of the film.[28,29] In such cases, the direction of the local surface normal can be used to describe silicon film formation (Figure 2b).

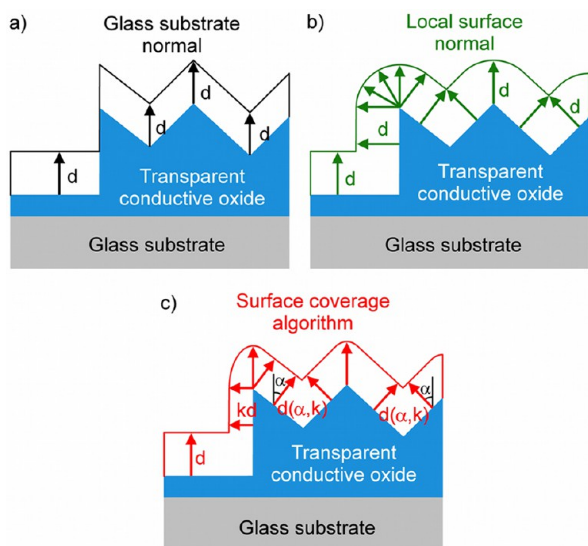

Figure 2. Modeling of silicon film formation (a) in the direction of glass substrate normal and (b) in the direction of local surface normal. (c) Developed surface coverage algorithm.

Figure 2a exhibits the commonly used approach in which the silicon film formation is determined by the direction of the glass substrate normal. The morphology of the film is an exact replica of the substrate morphology and there is no coverage of the substrate side walls. Realistic film morphologies can be obtained by using the direction of the local surface normal as shown in Figure 2b. This approach predicts differences between the substrate and the film

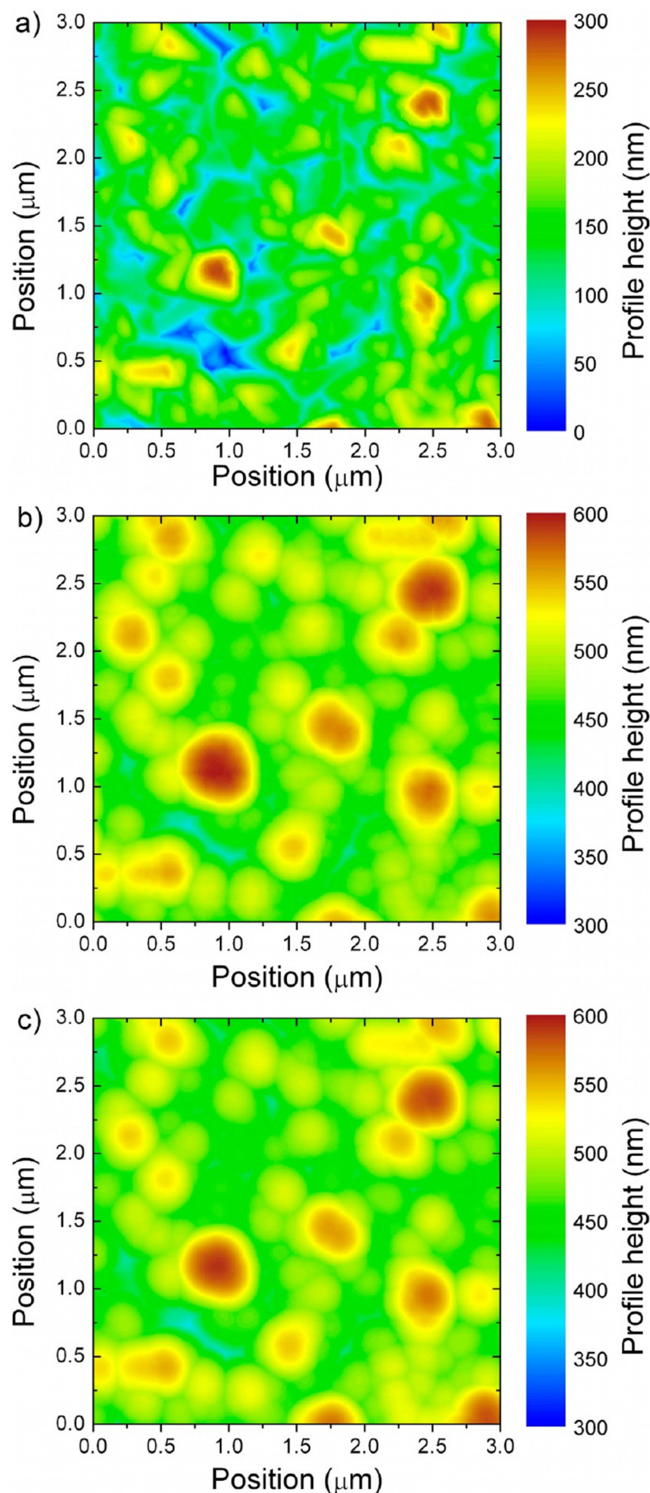

Figure 3. Atomic force microscopy images of (a) Asahi U substrate and (b) deposited 300 nm thick amorphous silicon film. (c) Calculated amorphous silicon film morphology deposited on Asahi U substrate.

morphology. Smoothening of the film surface occurs for substrate peak points and the film thickness for such peak points is equal to nominal film thickness (d). On the other hand, the film thickness for the substrate valley points is larger than the nominal film thickness. Hence, merging of the surface textures is possible for realistic film formation. To calculate realistic interface morphologies, a surface coverage algorithm is developed (Figure 2c). The surface coverage algorithm obtains interface morphology by determining the local surface normal for each substrate point and applying the film

dx.doi.org/10.1021/am401434y | ACS Appl. Mater. Interfaces 2013, 5, 7109−7116

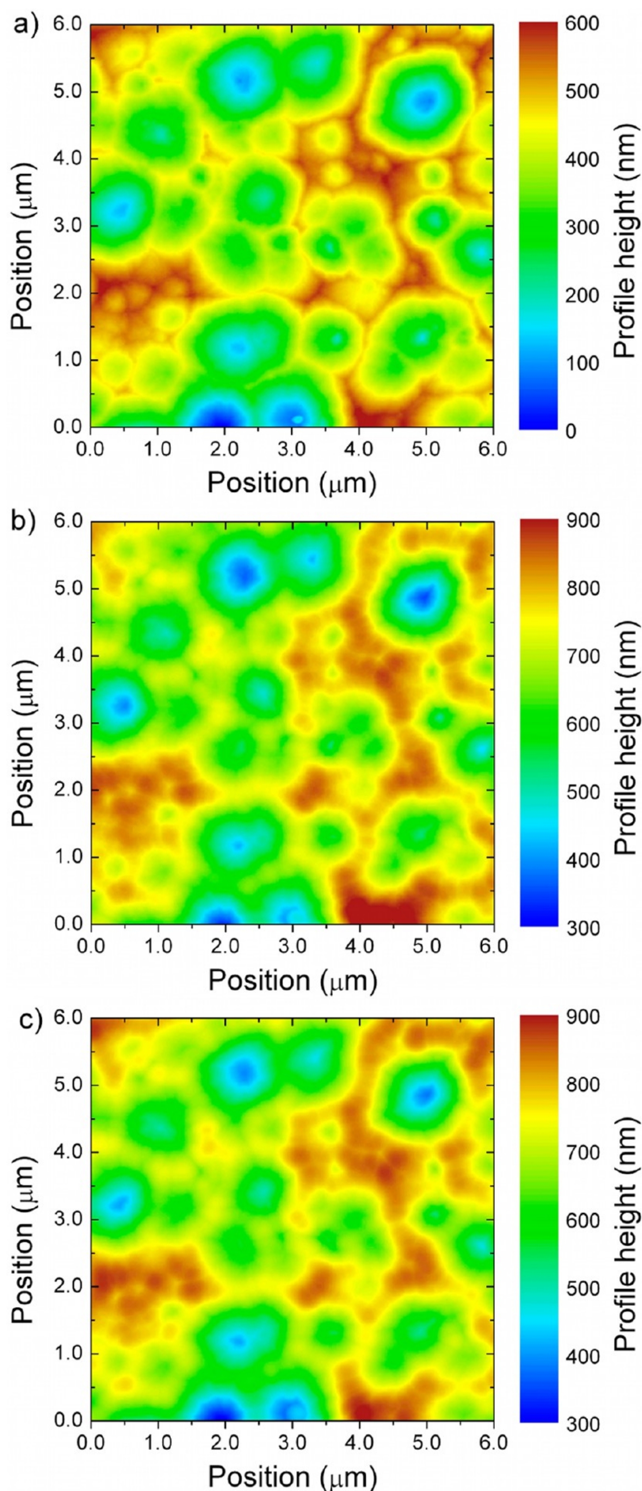

Figure 4. AFM images of (a) sputtered and wet-etched ZnO substrate and (b) deposited amorphous silicon film. (c) Calculated amorphous silicon film morphology on etched ZnO substrate.

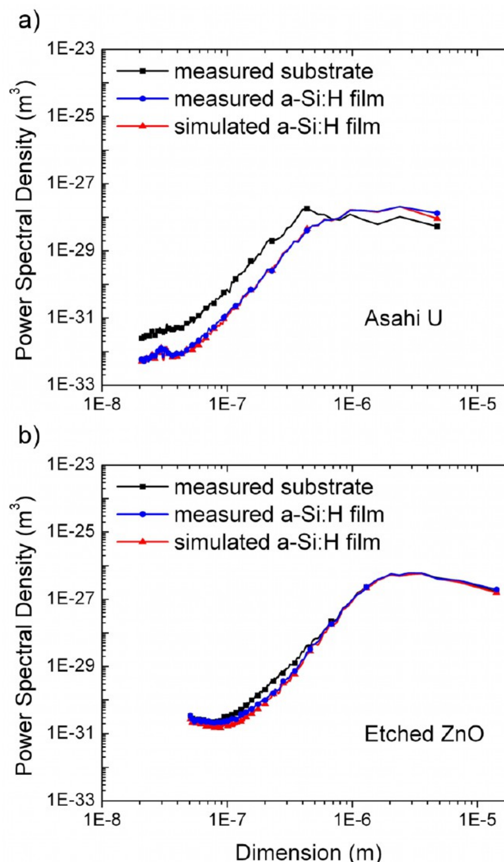

Figure 5. Power spectral density of the measured substrate (black line), amorphous silicon film (blue line), and calculated film morphology (red line) for (a) Asahi U and (b) wet-etched ZnO.

thickness in a given direction. The direction factor (k) is introduced assuming that the film thickness ($d(k, \alpha)$) depends upon the angle between the local surface normal and the glass substrate normal (α) as shown in Figure 2c. For substrate points where the local surface normal is parallel to the substrate normal ($\alpha = 0°$), the film thickness is equal to the nominal value. If the local surface normal is orthogonal to the glass substrate normal ($\alpha = 90°$), the film thickness is reduced to $k \cdot d$. When the direction factor is equal to zero, there is no surface coverage of the side walls, and film formation in the direction of the glass substrate normal is obtained (Figure 2a). If the direction factor is equal to one, the film thickness in the direction of the local surface normal is equal to the nominal value and a uniform film formation is achieved (Figure 2b). Depending on the substrate morphology, for some x- and y-coordinates several film surface points can be calculated, and the surface coverage algorithm selects the highest surface points. As a consequence, the developed surface coverage algorithm is not able to describe the formation of holes or voids in a film.

Experimental Setup. To verify the surface coverage algorithm, atomic force microscopy (AFM) was used to experimentally measure the front and back contact surface textures of silicon solar cells. In the first step, the surface of the TCO substrate is measured. For this study, Asahi U and etched ZnO films were chosen as substrates due to different surface textures. The Asahi U type substrates are characterized by the random arrangement of pyramids with lateral size in the range from 50 to 400 nm (Figures 3a and 6a). Etched ZnO films exhibit large and deep craters with lateral dimensions from 500 to 2000 nm (Figures 4a and 7a). Amorphous and microcrystalline silicon films were deposited on Asahi U and etched ZnO substrates by a PECVD process using a gas mixture of silane and hydrogen. The deposition of amorphous silicon was achieved at a deposition pressure of 133 Pa and for a substrate temperature of 260 °C. Microcrystalline silicon films were deposited at a pressure of 1333 Pa, and the substrate temperature was 200 °C. In the next step, the morphologies of the silicon films were measured. A special alignment process using laser markers was established to measure exactly the same area as for the substrates. In the last step, the morphologies of the silicon films were simulated. Only the AFM scans of the randomly textured TCO and the nominal thickness of deposited silicon films were used as input parameters for the surface coverage algorithm.

dx.doi.org/10.1021/am401434y | ACS Appl. Mater. Interfaces 2013, 5, 7109−7116

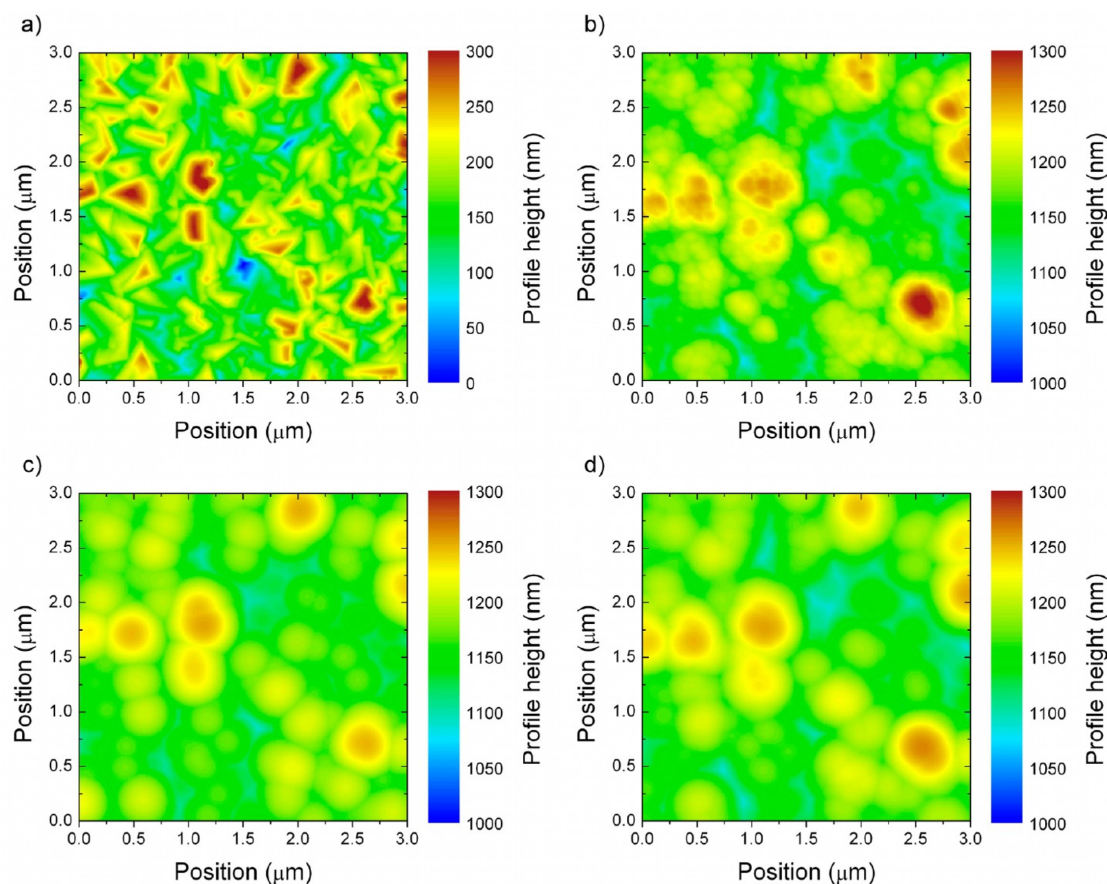

Figure 6. AFM images of (a) Asahi U substrate and (b) deposited 1000 nm thick microcrystalline silicon film. (c) Calculated microcrystalline silicon film morphology deposited on Asahi U substrate and (d) measured 1000 nm thick microcrystalline silicon film without nanofeatures.

RESULTS AND DISCUSSION

Amorphous Silicon Films. Amorphous silicon solar cells prepared on randomly textured substrates exhibit conversion efficiencies of more than 10%.[6,7] The typical thickness of amorphous silicon solar cells is 300 nm to achieve a good collection of photogenerated charge carriers.[3,5,6] Therefore, in this study, the nominal thickness of amorphous silicon films was 300 nm (Figures 3b and 4b). Amorphous silicon films exhibit uniform surface coverage, and to simulate film morphologies, the direction factor was set to one.

Figure 3a exhibits the AFM image of an Asahi U substrate, while the corresponding back contact morphology of a 300 nm thick amorphous silicon film is shown in Figure 3b. The calculated amorphous silicon film morphology is depicted in Figure 3c. A very good agreement between the measured and the simulated surface is observed. The measured and simulated silicon film morphologies reveal that lateral dimensions of pyramidal textures become larger after the deposition of amorphous silicon film. Smaller surface features disappear and merge with larger features if the lateral dimensions are smaller than the thickness of amorphous silicon film. Furthermore, a smoothening of the pyramid tips is observed.

Figure 4a exhibits an AFM scan of a sputtered and wet-etched ZnO substrate. The measured and simulated morphology of a 300 nm thick deposited amorphous silicon film are shown in Figure 4b and c, respectively. Again, the predicted surface morphology of amorphous silicon film is in good agreement with experimental data. Unlike Asahi U substrate, the lateral dimension of crater textures is almost the same after silicon film deposition. The surface textures of the etched ZnO do not merge since the lateral dimension of the craters is comparable with amorphous silicon film thickness. However, sharp edges around craters become smoother and rounder. In order to compare the measured and calculated silicon film morphologies, the power spectral density (PSD) was calculated and presented in Figure 5.

The PSD of the measured AFM images and simulated surface morphologies were obtained by a Fourier transform of the autocorrelation function.[31] Figure 5a exhibits the PSD of the measured Asahi U substrate (black line) and deposited amorphous silicon film (blue line). Differences in the PSD of the measured substrate and silicon film for Asahi U substrate confirm that the surface morphology is significantly influenced by the silicon film growth. Figure 5b presents the PSD of the measured ZnO substrate (black line) and deposited amorphous silicon film (blue line). The PSD of the etched ZnO substrate and the deposited silicon film exhibit only small differences. The detailed analysis of the Asahi U and etched ZnO surface textures shows that a larger change of the silicon film surface morphology is observed if the lateral dimensions of the surface texture are comparable or smaller than the silicon film thickness, which is the case for the Asahi U substrate. A comparison of the PSD for the measured (blue line) and calculated surfaces (red line) of the amorphous silicon film exhibits very good agreement for all spatial frequencies for both substrates.

dx.doi.org/10.1021/am401434y | *ACS Appl. Mater. Interfaces* 2013, 5, 7109−7116

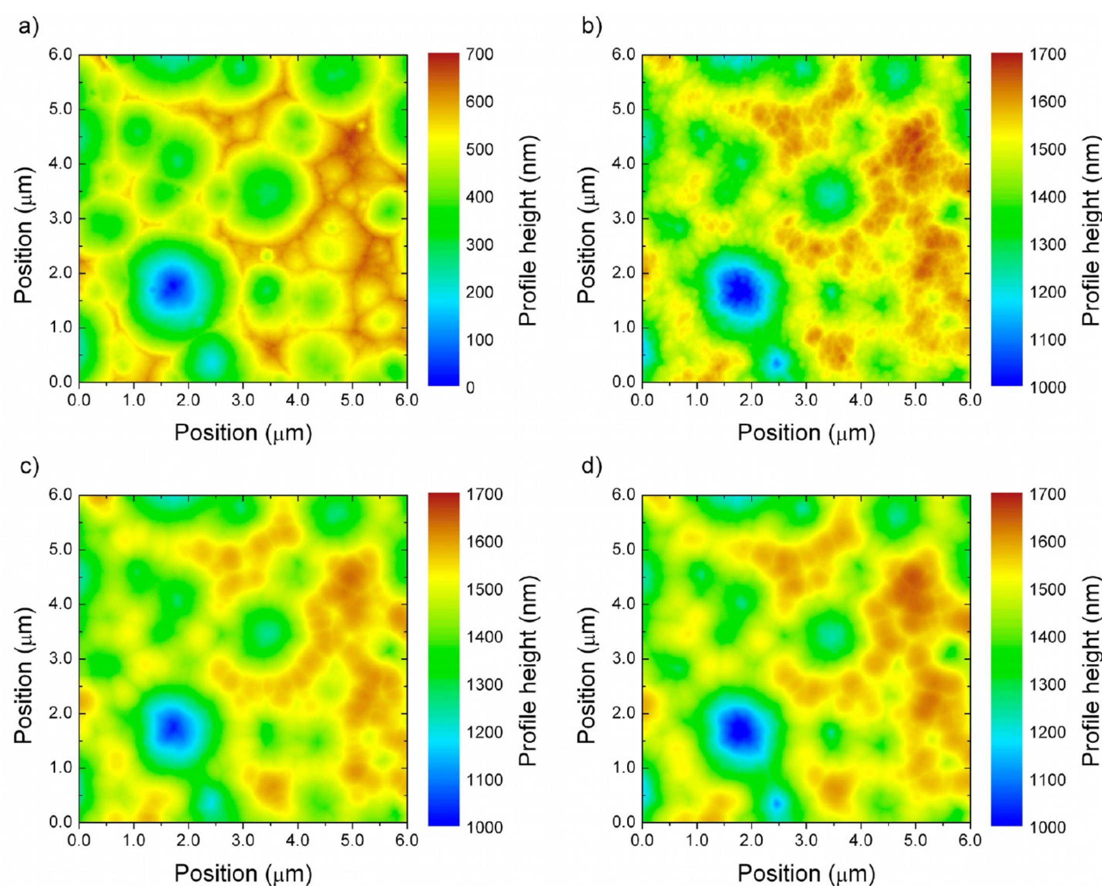

Figure 7. AFM images of (a) sputtered and wet-etched ZnO substrate and (b) deposited 1000 nm thick microcrystalline silicon film. (c) Calculated microcrystalline silicon film morphology on etched ZnO substrate and (d) measured 1000 nm thick microcrystalline silicon film without nanofeatures.

Microcrystalline Silicon Films. Microcrystalline silicon solar cells prepared on randomly textured substrates exhibit conversion efficiencies of more than 9% and short circuit currents exceeding 24 mA/cm^2.[2,6,7] Recently, microcrystalline silicon solar cells with a conversion efficiency of 10.5% and a short circuit current of 26.6 mA/cm^2 have been reported.[9] The formation of microcrystalline silicon films is a complex process. Growth of the microcrystalline silicon film is directional due to the formation of micro/nanocrystallites.[30] Consequently, the back contact surface textures are influenced by the film formation and by natural textures of the microcrystalline silicon. The nominal thickness of the deposited microcrystalline silicon film was 1000 nm. The film thickness of 1000 nm was chosen to be consistent with the thickness of a typical single junction microcrystalline silicon solar cell.[5,6] The surface coverage algorithm does not describe the formation of the microcrystalline silicon natural textures. Therefore, the algorithm was used only to describe the evolution of the front contact textures. The direction factor (k) was set to 0.75 accounting for the directional growth of the microcrystalline silicon films.

Figure 6a exhibits the AFM image of an Asahi U substrate, while the corresponding back contact morphology of a 1000 nm thick microcrystalline silicon film is shown in Figure 6b. The back contact morphology of microcrystalline silicon films can be described as a superposition of the front contact textures that propagate through microcrystalline silicon film and nanofeatures that are formed during film growth. The simulated morphology of microcrystalline silicon deposited on an Asahi U substrate is shown in Figure 6c. In order to allow for a direct comparison of measured and simulated data, the nanofeatures were filtered out.[32] Figure 6d shows the measured back contact morphology after filtering out the natural texture. Figure 6d exhibits good agreement with the simulated back contact morphology (Figure 6c). Consequently, the surface coverage algorithm is able to accurately predict the evolution of the front contact features for microcrystalline silicon film. Figure 6c and d show that back contact textures are larger and smoother compared to the substrate textures similar to amorphous silicon.

The measured morphology of etched ZnO substrate and deposited microcrystalline silicon film are presented in Figure 7a and b, respectively. Changes to the surface textures are much smaller compared to Asahi U substrate. However, the back contact morphology is again influenced by the microcrystalline silicon nanofeatures. The simulated back contact morphology is shown in Figure 7c. The measured back contact morphology without nanofeatures is presented in Figure 7d. A good agreement between the simulated and measured morphology is observed. A detailed comparison of the measured and simulated morphologies for both substrates is achieved by obtaining the PSD (Figure 8)

Figure 8a exhibits the PSD of the Asahi U substrate (black line) and deposited microcrystalline silicon film (blue line). Significant differences between the substrate and film morphology are observed similar to the amorphous silicon film. Figure 8a also shows the PSD for the simulated microcrystalline silicon film morphology (red line) and the measured film morphology

dx.doi.org/10.1021/am401434y | ACS Appl. Mater. Interfaces 2013, 5, 7109−7116

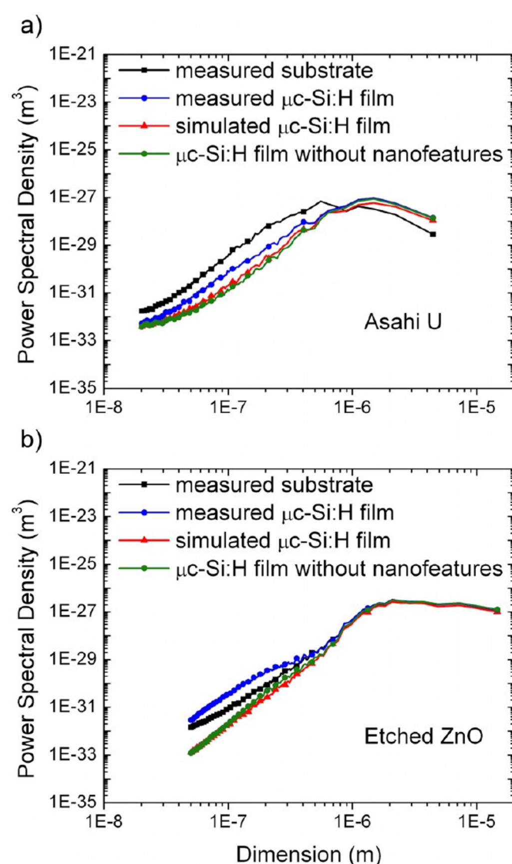

Figure 8. Power spectral density of the measured substrate (black line), microcrystalline silicon film (blue line), microcrystalline film without nanofeatures (green line), and calculated film morphology (red line) for (a) Asahi U and (b) wet-etched ZnO.

without nanofeatures (green line). The surface coverage algorithm accurately predicts the evolution of the front contact textures, and there are only small differences compared to the measured film without nanofeatures. The PSD of the measured morphologies of the etched ZnO substrate (black line) and corresponding microcrystalline silicon film (blue line) are shown in Figure 8b. The measured microcrystalline silicon film is significantly different from the substrate morphology, which is caused by the formation of nanofeatures. Nevertheless, the simulated film morphology (red line) is in good agreement with the measured film morphology without nanofeatures (green line).

Interface Morphology of Micromorph Tandem Solar Cells. Nowadays, the majority of research and production is focused on micromorph tandem solar cells.[4−8] Energy conversion efficiencies larger than 14% have been demonstrated for micromorph tandem solar cells.[6] To gain insight into light-trapping in micromorph tandem solar cells, the surface coverage algorithm was used to determine the interface morphologies and characterize changes to surface textures. The interface profiles and back contact morphology depend on the substrate type and the thicknesses of the top and bottom solar cell. For the Asahi U substrate, the thickness of the top cell ranges from 200 to 300 nm, while the thickness of the bottom cell is from 1300 to 1700 nm.[4−8] For the etched ZnO substrate, the thickness of the top cell is larger (300−400 nm) and the thickness of the bottom cell is smaller (800−1200 nm).[4−8]

Figure 9 exhibits simulated cross sections and changes to the roughness and surface feature size of tandem solar cells deposited on Asahi U and etched ZnO substrate. The average feature size was extracted using an image segmentation approach.[33] The cross section of tandem solar cell on an Ashai U-type substrate is shown in Figure 9a. The simulated thickness of the top cell was 250 nm, while the bottom cell was 1500 nm thick. The Asahi U substrate exhibits root mean square (RMS) roughness of ∼40 nm and an average feature size of ∼220 nm. Therefore, the Asahi U substrate efficiently scatters shorter wavelength light and a relatively thin amorphous silicon top cell is needed. On the other hand, longer wavelengths are not efficiently scattered and a thick bottom microcrystalline silicon solar cell is required. Consequently, the back contact morphology is smooth and exhibits poor light scattering properties. Figure 9c exhibits simulated RMS roughness and feature size of the back contact as a function of the solar cell thickness for amorphous, microcrystalline, and micromorph tandem silicon solar cells deposited on the Asahi U substrate. The lowest RMS roughness of the back contact and the largest back contact feature size are observed in the case of amorphous silicon. On the other hand, microcrystalline silicon solar cell will exhibit the highest RMS roughness and the smallest feature size of the back contact. Due to the small top cell thickness and large bottom cell thickness, the back contact morphology of tandem solar cells on Asahi U substrate is similar to microcrystalline silicon solar cells. For the top cell of 250 nm and bottom cell of 1500 nm, the back contact roughness drops to ∼30 nm, while the average feature size is increased to ∼540 nm. The cross section of a tandem solar cell on an etched ZnO substrate is shown in Figure 9b. The simulated thickness of the amorphous top cell was 350 nm, while the bottom cell was 1000 nm thick. The etched ZnO substrate exhibits RMS roughness of ∼100 nm and an average feature size of ∼840 nm. The textures of etched ZnO efficiently scatter/diffract longer wavelengths, but light-trapping properties for the shorter wavelengths are poor. Consequently, the top cell must be thicker than for the Asahi U substrate and the bottom cell must be thinner. The initial roughness and textures of the etched ZnO are much larger than for the Asahi U substrate. Hence, the back contact morphology is rough and efficiently scatters/diffracts longer wavelengths. Figure 9d exhibits simulated RMS roughness and feature size of the back contact for silicon solar cells deposited on etched ZnO substrate. As for Asahi U substrate, the lowest RMS roughness and largest feature size is observed for amorphous silicon. The back contact morphology of micromorph tandem solar cells is different from microcrystalline silicon since the bottom cell thickness is much smaller than for Asahi U substrate. For the top cell of 350 nm and bottom cell of 1000 nm, the back contact roughness drops to ∼87 nm while the feature size is increased to ∼975 nm.

The surface coverage algorithm does not describe the formation of microcrystalline natural textures and the cross sections shown in Figure 9 exhibit back contact morphology without nanofeatures. Also, the influence of nanofeatures on the back contact roughness and feature size was neglected. The nanofeatures of the back contact can have a significant influence on the light trapping and optical losses of the back contact.[34,35] In order to get a better description of the microcrystalline and micromorph tandem silicon solar cell, artificial nanotextures can be added to the simulated back contact morphologies.[35]

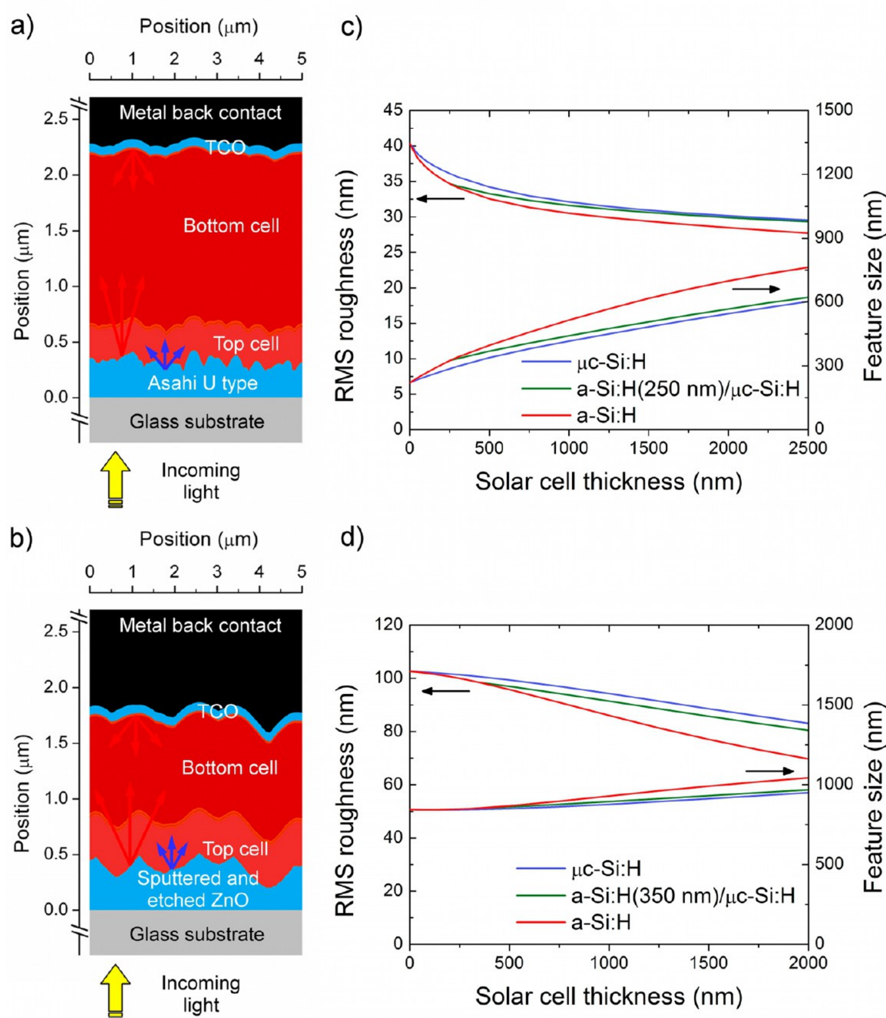

Figure 9. Cross sections of micromorph tandem solar cells prepared on (a) Asahi U type substrate and (b) etched ZnO substrate. Root mean square roughness and surface feature size as a function of a solar cell thickness for (c) Asahi U type substrate and (d) etched ZnO substrate.

CONCLUSION

A simple approach to predict the surface of silicon solar cells prepared on the random textured substrates is presented and compared to experimental data. The prediction model was demonstrated for amorphous and microcrystalline silicon films prepared on Asahi U and etched ZnO substrates. The morphology of silicon thin films was calculated by using the AFM scan of the TCO substrate and the thickness of the silicon film as input data. The low temperature amorphous silicon grows uniformly in the direction of the local surface normal. The simulated amorphous silicon film morphologies are in good agreement with the measured data for both substrates. The growth of microcrystalline silicon is a complex process resulting in different surface morphologies compared to amorphous silicon. To account for the more directional formation of the microcrystalline silicon film, a direction factor was introduced. The surface coverage algorithm accurately predicts the evolution of the front contact textures, and the simulated microcrystalline silicon film morphologies are in good agreement with measured films without nanofeatures. An accurate description of the interface morphologies provides better insights in the optics of silicon solar cells and allows for determining optimal light trapping structures. The developed surface coverage algorithm is necessary to understand light trapping in silicon single junction and micromorph tandem solar cells. The presented algorithm is not limited to randomly textured substrates and should also be used to determine realistic interface morphologies of silicon solar cells prepared on arbitrary textured substrates, including nanowire or textured glass substrates.

AUTHOR INFORMATION

Corresponding Author

*E-mail: d.knipp@jacobs-university.de.

Notes

The authors declare no competing financial interest.

REFERENCES

(1) Hongsingthong, A.; Krajangsang, T.; Yunaz, I. A.; Miyajima, S.; Konagai, M. *Appl. Phys. Express* **2010**, 3, 051102−1−3.

(2) Faÿ, S.; Kroll, U.; Bucher, C.; Vallat-Sauvain, E.; Shah, A. *Sol. Energy Mater. Sol. Cells* **2005**, *86* (3), 385−397.

(3) Palanchoke, U.; Jovanov, V.; Kurz, H.; Obermeyer, P.; Stiebig, H.; Knipp, D. *Opt. Express* **2012**, *20* (6), 6340−6347.

(4) Krc, J.; Lipovsek, B.; Bokalic, M.; Campa, A.; Oyama, T.; Kambe, M.; Matsui, T.; Sai, H.; Kondo, M.; Topic, M. *Thin Solid Films* **2010**, *518* (11), 3054−3058.

(5) Müller, J.; Rech, B.; Springer, J.; Vanecek, M. *Sol. Energy* **2004**, *77* (6), 917−930.
(6) Konagai, M. *Jpn. J. Appl. Phys.* **2011**, *50*, 030001−1−12.
(7) Rech, B.; Repmann, T.; van den Donker, M. N.; Berginski, M.; Kilper, T.; Hüpkes, J.; Calnan, S.; Stiebig, H.; Wieder, S. *Thin Solid Films* **2006**, *511−512*, 548−555.
(8) Ding, K.; Kirchartz, T.; Pieters, B. E.; Ulbrich, C.; Ermes, A. M.; Schicho, S.; Lambertz, A.; Carius, R.; Rau, U. *Sol. Energy Mater. Sol. Cells* **2011**, *95* (12), 3318−3327.
(9) Hänni, S.; Alexander, D. T. L.; Ding, L.; Bugnon, G.; Boccard, M.; Battaglia, C.; Cuony, P.; Escarré, J.; Parascandolo, G.; Nicolay, S.; Cantoni, M.; Despeisse, M.; Meillaud, F.; Ballif, C. *IEEE J. Photovoltaics* **2013**, *3* (1), 11−16.
(10) Berginski, M.; Hüpkes, J.; Gordijn, A.; Reetz, W.; Wätjen, T.; Rech, B.; Wuttig, M. *Sol. Energy Mater. Sol. Cells* **2008**, *92* (9), 1037−1042.
(11) Haug, F.-J.; Söderström, T.; Python, M.; Terrazzoni-Daudrix, V.; Niquille, X.; Ballif, C. *Sol. Energy Mater. Sol. Cells* **2009**, *93* (6−7), 884−887.
(12) Sai, H.; Fujiwara, H.; Kondo, M.; Kanamori, Y. *Appl. Phys. Lett.* **2008**, *93* (14), 143501−1−3.
(13) Ferry, V. E.; Verschuuren, M. A.; Li, H. B. T.; Verhagen, E.; Walters, R. J.; Schropp, R. E. I.; Atwater, H. A.; Polman, A. *Opt. Express* **2010**, *18* (S2), A237−A245.
(14) Sai, H.; Jia, H.; Kondo, M. *J. Appl. Phys.* **2010**, *108* (4), 044505−1−9.
(15) Yamamoto, K. *IEEE Trans. Electron Devices* **1999**, *46* (10), 2041−2047.
(16) Yue, G.; Sivec, L.; Owens-Mawson, J.; Yan, B.; Yang, J.; Guha, S. *Appl. Phys. Lett.* **2009**, *95* (26), 263501−1−3.
(17) Yan, B.; Yue, G.; Sivec, L.; Owens-Mawson, J.; Yang, J.; Guha, S. *Sol. Energy. Mater. Sol. Cells* **2012**, *104*, 13−17.
(18) Madzharov, D.; Dewan, R.; Knipp, D. *Opt. Express* **2011**, *19* (S2), A95−A107.
(19) Ferry, V. E.; Polman, A.; Atwater, H. A. *ACS Nano* **2011**, *5* (12), 10055−10064.
(20) Lacombe, J.; Sergeev, O.; Chakanga, K.; von Maydell, K.; Agert, C. *J. Appl. Phys.* **2011**, *110* (2), 023102−1−6.
(21) Rockstuhl, C.; Fahr, S.; Lederer, F.; Bittkau, K.; Beckers, T.; Carius, R. *Appl. Phys. Lett.* **2008**, *93* (6), 061105−1−3.
(22) Vanecek, M.; Babchenko, O.; Purkrt, A.; Holovsky, J.; Neykova, N.; Poruba, A.; Remes, Z.; Meier, J.; Kroll, U. *Appl. Phys. Lett.* **2011**, *98* (16), 163503−1−3.
(23) Solntsev, S.; Isabella, O.; Caratelli, D.; Zeman, M. *IEEE J. Photovoltaics* **2013**, *3* (1), 46−52.
(24) Hsu, C.-M.; Battaglia, C.; Pahud, C.; Ruan, Z.; Haug, F.-J.; Fan, S.; Ballif, C.; Cui, Y. *Adv. Energy Mater.* **2012**, *2* (6), 628−633.
(25) Nam, W. J.; Ji, L.; Benanti, T. L.; Varadan, V. V.; Wagner, S.; Wang, Q.; Nemeth, W.; Neidich, D.; Fonash, S. J. *Appl. Phys. Lett.* **2011**, *99* (7), 073113−1−3.
(26) Sai, H.; Saito, K.; Hozuki, N.; Kondo, M. *Appl. Phys. Lett.* **2013**, *102* (5), 053509−1−5.
(27) Battaglia, C.; Hsu, C.-M.; Söderström, K.; Escarré, J.; Haug, F.-J.; Charrière, M.; Boccard, M.; Despeisse, M.; Alexander, D. T. L.; Cantoni, M.; Cui, Y.; Ballif, C. *ACS Nano* **2012**, *6* (3), 2790−2797.
(28) Tsai, C. C.; Knights, J. C.; Chang, G.; Wacker, B. *J. Appl. Phys.* **1986**, *59* (8), 2998−3001.
(29) Street, R. A. *Hydrogenated Amorphous Silicon*; Cambridge University Press, Cambridge, 1991, Chapter 2.
(30) Collins, R. W.; Ferlauto, A. S.; Ferreira, G. M.; Chen, C.; Koh, J.; Koval, R. J.; Lee, Y.; Pearce, J. M.; Wronski, C. R. *Sol. Energy. Mater. Sol. Cells* **2003**, *78* (1−4), 143−180.
(31) Duparre, A.; Borrull, J. F.; Gliech, S.; Notni, G.; Steinert, J.; Bennett, J. M. *Appl. Opt.* **2002**, *41* (1), 154−171.
(32) Liu, J. G. *Int. J. Remote Sensing* **2000**, *21* (18), 3461−3472.
(33) Dewan, R.; Owen, J. I.; Madzharov, D.; Jovanov, V.; Hupkes, J.; Knipp, D. *Appl. Phys. Lett.* **2012**, *101* (10), 103903−1−4.
(34) Palanchoke, U.; Jovanov, V.; Kurz, H.; Dewan, R.; Magnus, P.; Stiebig, H.; Knipp, D. *Appl. Phys. Lett.* **2013**, *102* (8), 083501−1−3.
(35) Jovanov, V.; Palanchoke, U.; Magnus, P.; Stiebig, H.; Knipp, D. *Sol. Energy Mater. Sol. Cells* **2013**, *110*, 49−57.